Coupled-Cluster and Many-Body Perturbation Study of Energies, Structures, and Phonon Dispersions of Solid Hydrogen Fluoride

OLASENI SODE,[1] MURAT KEÇELI,[2] SO HIRATA,[1,2] KIYOSHI YAGI[3]

[1]*Department of Chemistry, Quantum Theory Project, The Center for Macromolecular Science and Engineering, University of Florida, Gainesville, FL 32611-8435*

[2]*Department of Physics, Quantum Theory Project, The Center for Macromolecular Science and Engineering, University of Florida, Gainesville, FL 32611-8435*

[3]*Department of Applied Chemistry, School of Engineering, The University of Tokyo, Tokyo 113-8656, Japan*

Received 3 October 2008; accepted 24 November 2008
Published online 4 February 2009 in Wiley InterScience (www.interscience.wiley.com).
DOI 10.1002/qua.22022

ABSTRACT: A linear-scaling electron-correlation method based on a truncated many-body expansion of the energies of molecular crystals has been applied to solid hydrogen fluoride. The energies, structures, harmonic, and anharmonic frequencies of the infrared- and/or Raman-active vibrations, phonon dispersions, and inelastic neutron scattering (INS) of the solid have been simulated employing an infinite, periodic, one-dimensional zigzag hydrogen-bonded chain model. The Hartree–Fock, second-order Møller–Plesset (MP2), coupled-cluster singles and doubles (CCSD), and CCSD with a noniterative triples correction [CCSD(T)] methods have been combined with the aug-cc-pVDZ and aug-cc-pVTZ basis sets and, in some instances, the counterpoise corrections of the basis-set superposition errors. The computed structural parameters agree with the observed within 0.1–0.2 Å and a few degrees, and the anharmonic frequencies obtained by vibrational MP2 allowing two-phonon couplings reproduce the observed frequencies

Correspondence to: S. Hirata; e-mail: hirata@qtp.ufl.edu

Dedicated to Professor Kimihiko Hirao on the occasion of his retirement from The University of Tokyo.

Contract grant sponsor: U.S. Department of Energy, Office of Science, Office of Basic Energy Sciences.
Contract grant number: DE-FG02-04ER15621.
Contract grant sponsor: Donors of the American Chemical Society Petroleum Research Fund.
Contract grant number: 48440-AC6.

semiquantitatively if the potential energy surface is obtained by a correlated theory. They support the revised infrared and Raman band assignments of librational modes made by Hirata and Iwata (J Phys Chem A 1998, 102, 8426) and provide more detailed assignments of the observed INS features. Int J Quantum Chem 109: 1928–1939, 2009

Key words: coupled-cluster theory; perturbation theory; molecular crystals; inelastic neutron scattering; phonon dispersions

Introduction

The inability of ab initio electron-correlation methods to treat (crystalline or amorphous) solids is one of the chief shortcomings of modern electronic structure theory [1]. The sheer high dimension of the equation of motion together with the presence of many interaction types (covalent, ionic, hydrogen, van der Waals, etc.) in such systems makes electron-correlation methods nonscalable with the system size and expensive to apply. A straightforward application of electronic structure theory to periodic solids—crystalline orbital (CO) theory [2–6]—has been useful for polymers, but calculations beyond Hartree–Fock (HF) or density-functional theoretical (DFT) levels have not been routine and the corresponding methods (e.g., Ref. [7]) are also tedious to implement even for polymers let alone for slabs and solids.

The most effective technique of reducing the dimension of partial differential equations is the (approximate) separation of variables. When a solid or cluster is composed of weakly-interacting subunits, the total Hamiltonian and wave function are approximately additively and multiplicatively separable, respectively, breaking down a high-dimensional Schrödinger equation into several, low-dimensional equations, which are much easier to solve. As the electronic Hamiltonian consists of one- and two-body operators, the elementary unit of separation should be overlapping dimers as well as monomers. Hence, the total energy of such systems can be approximated accurately by a many-body expansion truncated after the two-body term [8, 9]:

$$E = \sum_i E_i + \sum_{i<j} (E_{ij} - E_i - E_j), \qquad (1)$$

where E_i and E_{ij} are the energies of the ith monomer and of dimer consisting of the ith and jth monomers. Because the longest-range chemical interaction between subunits in a nonmetallic solid or cluster is of classical Coulomb (charge-charge, dipole-dipole, etc.) type, these energies should be assessed in the framework of atomic partial charges [9] or molecular dipole moments [8] that make up the electrostatic field of the rest of the solid or cluster constituents. Because this field is affected by the dimer or monomer as much as the former affects the latter, self-consistency must be attained for the field first before the quantum-mechanical terms are evaluated.

We have devised a fast method for molecular clusters and molecular crystals based on these ideas [8–10]. It first determines the self-consistent atomic partial charges and/or self-consistent dipole moments of subunits (at the HF level) in an iterative algorithm. It subsequently evaluates the energies of dimers and monomers in Eq. (1) in the field created by the other subunits' charges or dipoles. Our method has at least the following seven unique merits:

1. Achieves high accuracy at the lowest-order (i.e., binary-interaction) approximation, treating intramolecular bonds of any type and intermolecular bonds of ionic, hydrogen-bond, and van der Waals types accurately;
2. Forms a systematic hierarchy of cost-accuracy trade-off, namely, binary-, ternary-, and quaternary-interaction methods, etc.;
3. A low cost-scaling (quadratic scaling for small clusters and linear scaling for large clusters and solids);
4. Lends itself to straightforward function counterpoise basis-set superposition error (BSSE) corrections;
5. A low implementation cost (only a short script that executes an unmodified electronic structure code needs to be written);
6. Yields size-extensive energies irrespective of the underlying electron-correlation treatments;
7. Readily extensible to (analytical) gradients and Hessians and other properties such as electronic excitations.

The applications of this method are, however, at present limited to clusters and crystals of molecules that are only weakly interacting through hydrogen bonds or van der Waals interactions. Furthermore, a tacit assumption is made that each molecule is unambiguously assignable with an integer electron count.

In this article, we apply this method to solid hydrogen fluoride, which is one of the most thoroughly characterized hydrogen-bonded crystals both experimentally and theoretically and is, therefore, an ideal system to assess the performance of this new method. The solid is known for its strong anisotropy caused by the one-dimensional hydrogen-bond network [11–13]. We have, therefore, modeled it as a single zigzag chain of $(HF)_n$ and $(DF)_n$ with two molecules in a translational repeat unit. We have combined the method with the periodic boundary conditions and examined the structures, energies, and infrared- and/or Raman-active phonons, along with phonon dispersion curves and inelastic neutron scattering (INS) from the solid. The ability to handle phonons with nonzero linear momenta as easily as zone-center phonons is another advantage of our "energy-based" method, which is only loosely coupled with the periodic boundary conditions, in contrast to the CO theory. We have employed HF, second-order Møller–Plesset perturbation (MP2), coupled-cluster singles and doubles (CCSD), and CCSD with a noniterative triples correction [CCSD(T)] methods with the inclusion, in some instances, counterpoise BSSE corrections. These correlated treatments, along with the long-range Coulomb lattice sums with self-consistent electrostatic fields, should adequately capture the hydrogen-bond cooperativity [14–20], which is essential to quantitatively describing molecular crystals. Furthermore, anharmonic frequencies of the zone-center phonons have also been computed by vibrational MP2 [21–23], taking account of the anharmonic couplings of up to two modes [24], and are compared with the frequencies of the observed infrared and/or Raman bands.

Computational Methods

In the binary-interaction method [10], the energy per unit cell of a one-dimensional periodic system is approximated by the following equation:

$$E_{\text{cell}} = \sum_{i<j}(E_{i(0)j(0)} - E_{i(0)} - E_{j(0)}) + \frac{1}{2}\sum_{n=-S}^{S}(1 - \delta_{n0})\sum_{i,j}(E_{i(0)j(n)} - E_{i(0)} - E_{j(n)}) + \sum_{i}E_{i(0)}, \quad (2)$$

where $E_{i(0)j(n)}$ denotes the energy of the dimer consisting of the ith molecule in the central cell and jth molecule in the nth cell, $E_{j(n)}$ the energy of the jth monomer in the nth cell, and δ_{n0} is Kronecker's delta. The integer parameters S, M, and L determine the cutoff radii for the short-, mid-, and long-range interaction terms, respectively. The dimer and monomer energies are obtained by an (unmodified) electronic structure program (such as Q-CHEM [25] or NWCHEM [26]). However, as mentioned previously, they are not calculated in vacuums but in the presence of the electrostatic field surrounding them. Thus, the Hamiltonian of the dimers and monomers includes the potential,

$$V(\mathbf{r}) = \sum_{m=-L}^{-M-1} V_m^{\text{LR}}(\mathbf{r}) + \sum_{m=-M}^{M} V_m^{\text{MR}}(\mathbf{r}) + \sum_{m=M+1}^{L} V_m^{\text{LR}}(\mathbf{r}), \quad (3)$$

of which the mid-range (MR) part is expressed by

$$V_m^{\text{MR}}(\mathbf{r}) = \sum_k \sum_\gamma \frac{q_\gamma^k}{|\mathbf{r} - \mathbf{r}_\gamma^{k(m)}|}, \quad (4)$$

where q_γ^k represents the self-consistently determined partial charge of atom "γ" in the kth molecule in the mth unit cell centered at $\mathbf{r}_\gamma^{k(m)}$. In the case where the atom is in the dimer being calculated, this value becomes zero. The long-range (LR) part is a sum of the potentials created by the dipole moments of unit cells:

$$V_m^{\text{LR}}(\mathbf{r}) = \frac{q}{|\mathbf{r} - \mathbf{r}_m + \frac{1}{2}\mathbf{d}|} - \frac{q}{|\mathbf{r} - \mathbf{r}_m - \frac{1}{2}\mathbf{d}|}, \quad (5)$$

where $q\mathbf{d}$ is the self-consistently determined dipole moment of a unit cell.

The energy gradients and Hessians can also be obtained approximately by

$$\frac{\partial E_{\text{cell}}}{\partial x} = \sum_{i<j}\left\{\frac{\partial E_{i(0)j(0)}}{\partial x} - \frac{\partial E_{i(0)}}{\partial x} - \frac{\partial E_{j(0)}}{\partial x}\right\} + \frac{1}{2}\sum_{n=-S}^{S}(1 - \delta_{n0})\sum_{i,j}\left\{\frac{\partial E_{i(0)j(n)}}{\partial x} - \frac{\partial E_{i(0)}}{\partial x} - \frac{\partial E_{j(n)}}{\partial x}\right\} + \sum_{i}\frac{\partial E_{i(0)}}{\partial x}, \quad (6)$$

$$\frac{\partial^2 E_{\text{cell}}}{\partial x \partial y} = \sum_{i<j}\left\{\frac{\partial^2 E_{i(0)\,j(0)}}{\partial x \partial y} - \frac{\partial^2 E_{i(0)}}{\partial x \partial y} - \frac{\partial^2 E_{j(0)}}{\partial x \partial y}\right\} + \frac{1}{2}\sum_{n=-S}^{S}(1 - \delta_{n0})\sum_{i,j}\left\{\frac{\partial^2 E_{i(0)\,j(n)}}{\partial x \partial y} - \frac{\partial^2 E_{i(0)}}{\partial x \partial y} - \frac{\partial^2 E_{j(n)}}{\partial x \partial y}\right\} + \sum_{i}\frac{\partial^2 E_{i(0)}}{\partial x \partial y'}, \quad (7)$$

where x (y) is either an in-phase, collective coordinate of all atoms that are related by translational symmetry (including the lattice constant) or an individual coordinate of an atom. The gradients and Hessians with respect to in-phase coordinates are useful for geometry optimization and $k = 0$ phonons, whereas the Hessians with respect to individual atomic coordinates are needed for computing phonon dispersions. As the electrostatic field varies with atomic coordinates, fully accurate gradients and Hessians would have to account for these variations; however, it has been found that the effect of such variations is negligible and this approximation is sufficiently accurate [10, 27]. The one exception is the gradients with respect to the lattice constant [28]. With increasing the lattice constant, the distance between the outermost charges or dipoles and the central unit cell increases substantially, thus, creating a large energy difference with respect to a small displacement. The lattice gradient, therefore, includes a correction for this contribution as follows:

$$\frac{\partial E_{\text{cell}}}{\partial a} = \frac{1}{2}\sum_{n=-S}^{S}\sum_{i,j}\sum_{\gamma} n\left\{\frac{\partial E_{i(0)\,j(n)}}{\partial x_{\gamma}^{j(n)}} - \frac{\partial E_{j(n)}}{\partial x_{\gamma}^{j(n)}}\right\} + \frac{\partial E^{\text{MR}}}{\partial a} + \frac{\partial E^{\text{LR}}}{\partial a}, \quad (8)$$

where **a** is the lattice vector which is parallel to the chain axis (say, x) and $x_{\gamma}^{j(n)}$ is the x-coordinate of atom "γ" of the jth molecule in the nth cell and

$$E^{\text{MR}} = \frac{1}{2}\sum_{m=-M}^{M}(1 - \delta_{m0})\sum_{i,j}\sum_{\gamma,\eta}\frac{q_{\gamma}^{i} q_{\eta}^{j}}{|\mathbf{r}_{\gamma}^{i(0)} - \mathbf{r}_{\eta}^{j(m)}|}, \quad (9)$$

$$E^{\text{LR}} = \frac{1}{2}\sum_{m=-L}^{-M-1} E_m^{\text{LR}} + \frac{1}{2}\sum_{m=M+1}^{L} E_m^{\text{LR}}, \quad (10)$$

with

$$E_m^{\text{LR}} = q^2\frac{\mathbf{d}\cdot\mathbf{d} - 3(\mathbf{d}\cdot\hat{\mathbf{r}_m})^2}{\mathbf{r}_m^3}, \quad (11)$$

where $\mathbf{r}_m = m\mathbf{a}$.

The Boys–Bernardi function counterpoise BSSE correction [29] can be applied to energies, gradients, and Hessians by replacing the energy expression in Eq. (1) by the following and similarly in Eqs. (6), (7), and (8):

$$(E_{i(0)\,j(0)} - E_{i(0)} - E_{j(0)}) - (E_{i(0)\,j_G(0)} - E_{i(0)\,j_V(0)}) - (E_{i_G(0)\,j(0)} - E_{i_V(0)\,j(0)}), \quad (12)$$

where $E_{i(0)}$, $E_{i(0)\,j_G(0)}$, and $E_{i_V(0)\,j(0)}$ correspond to the dimers wherein the jth molecule in the central cell is replaced by self-consistent atomic charges, a ghost molecule (no atoms, no atomic charges, but with basis sets), and a void (no atoms, no atomic charges, and no basis sets), respectively.

Our method is a simplification of Kitaura's pair-interaction method [30] in that the necessity of the self-consistent electron density is eliminated in the former. For other related approaches, see Tschumper [31], Dahlke and Truhlar [32, 33], Li et al. [34], Jiang et al. [35], Stoll et al. [36], and Manby et al. [37]. For some recent accurate calculations of molecular crystals, see Podeszwa et al. [38] and Ringer and Sherrill [39].

Application: Solid Hydrogen Fluoride

BACKGROUND

The structures of solid hydrogen fluoride [$(HF)_n$] and deuterium fluoride [$(DF)_n$] have been well-characterized experimentally. The X-ray diffraction study of Atoji and Lipscomb [11] provided reliable bond lengths, bond angles, and lattice constants of the orthorhombic crystal. Giguère and Zengin [40] and Anderson et al. [41] investigated the infrared and Raman spectra of $(HF)_n$. These studies indicated that the crystal had a highly anisotropic structure composed of long zigzag chains with strong "cooperative behavior" provided by the linear hydrogen-bond network. The chain is known to both belong to the factor group isomorphous to C_{2v} and have four atoms (two molecules) in a translational repeat unit. Additional studies of the vibrational spectra [13, 42–45] and neutron diffraction and NMR studies [12, 46] have been performed. A consensus exists on the assignments of the high-frequency stretching modes and of the pseudotranslational modes [42], but the assignments of librational modes remain uncertain [47].

TABLE I

The structural parameters of $(HF)_n$ in Å and degrees.

	H-F bond length	H. . . F bond length	F. . . F bond length	FHF angle	FFF angle	Translational period
HF/aDZ[a]	0.913	1.75	2.66	177	134	4.89
MP2/aDZ[a]	0.947	1.63	2.57	176	118	4.41
CP-MP2/aDZ[a]	0.945	1.69	2.63	177	121	4.57
CCSD/aDZ[a]	0.941	1.64	2.58	177	125	4.58
HF/aTZ[a]	0.913	1.74	2.65	179	134	4.89
MP2/aTZ[a]	0.947	1.60	2.54	178	125	4.51
CP-MP2/aTZ[a]	0.943	1.64	2.58	175	120	4.48
Experiment[b]	0.97, 0.95	1.53	2.50, 2.49	176	116, 120.1	4.26, 4.32

[a] "aXZ" stands for the aug-cc-pVXZ basis set.
[b] References [11], [12], and [46].

Computational investigation of this solid is also quite vast. The CO calculations in the HF approximation by Beyer and Karpfen [48] and by Hirata and Iwata [47] produced qualitatively correct results, but significantly underestimated the hydrogen-bond cooperativity and were thus unable to provide a reliable basis of spectral band assignments. Some DFT models were also combined with the CO technique and were found to describe the cooperativity more accurately if a gradient-corrected exchange-correlation functional was used. On the basis of these calculations, assignments of the observed infrared and Raman bands (the $k = 0$ phonons) were suggested by Hirata and Iwata [47], revising some earlier assignments made by Anderson et al. [41], by Pinnick et al. [45], and by Kittelberger and Hornig [42]. These CO calculations were strongly based on the periodic boundary conditions and could probe only the $k = 0$ phonons, which did not disrupt periodicity.

The so-called incremental scheme enabled Buth and Paulus [49, 50] to apply CCSD to $(HF)_n$. They obtained an accurate binding energy of this solid in the complete-basis-set limit by extrapolation. Their method is similar to the one proposed here in the sense that they both are based on truncated many-body expansions of correlation energies, but they differ in several critical points. Buth and Paulus [49, 50] solved the HF part of the problem using the CO method and the subsequent correlation calculations employed localized (Wannier) functions. Because of this algorithmic complexity, only single-point calculations were possible. To the authors' knowledge, no geometry optimization nor vibrational analysis has been performed for $(HF)_n$ or $(DF)_n$ by an electron-correlation method.

STRUCTURES

The geometrical parameters of $(HF)_n$ were optimized at the HF, MP2, and CCSD levels with an additional BSSE corrected calculation at the MP2 level (CP-MP2). The truncation radii of the short- (*S*), mid- (*M*), and long-range (*L*) cutoffs were 50, 500, and 1,000 bohrs.

Table I compares our calculated structural parameters with the observed values obtained by Atoji and Lipscomb [11], by Johnson et al. [12], and by Habuda et al. [46]. The H—F bond length with the electron correlation calculations shows good agreement with the experimental results of 0.97 ± 0.02 Å and 0.95 ± 0.03 Å. The HF values of this bond length are significantly shorter than the observed. Large errors with the opposite sign are observed in the H. . .F and the F. . .F distances predicted by HF, which are overestimated by about 0.2 Å. The FHF angle observed by the neutron diffraction studies of Johnson et al. [12] is in agreement with all of our calculated angles. However, for the FFF angle, our values seem to deviate somewhat from experiments (116° and 120.1°), especially in the HF case (134°). At the MP2 level and above, the angles are greatly decreased. The HF values of the translational period (4.89 Å) are much too large as compared with those obtained by Johnson et al. (4.26 Å) [12] and by Atoji and Lipscomb (4.32 Å) [11] because of the overestimations of the H. . .F and the F. . .F distances and FFF angle at this level. The reasonable estimate of the observed values is reached at the CP-MP2/aug-cc-pVTZ level (4.48 Å).

The large disagreement at the HF level points to the fact that the theory is unsuitable at accurately predicting not only the crystal structure but more

TABLE II

The harmonic frequencies (in cm^{-1}) of the infrared- and/or Raman-active vibrations of $(HF)_n$.

Mode	HF/aDZ[a]	HF/aTZ[a]	MP2/aDZ[a]	CP-MP2/aDZ[a]	MP2/aTZ[a]	CP-MP2/ aTZ[a]	CCSD/ aDZ[a]	Infrared[b]	Raman[c]
$T(A_1)$	138	136	200	178	192	184	185	202	188
$T(B_1)$	276	274	329	294	344	310	305	356	364
$L(A_1)$	523	543	563	545	633	570	537	553	569
$L(A_2)$	567	571	628	585	679	613	597	Inactive	687
$L(B_2)$	587	595	681	631	683	660	655	792	742
$L(B_1)$	769	785	1,002	931	972	965	953	975-1,025	943
$S(A_1)$	4,106	4,102	3,535	3,610	3,539	3,622	3,686	3,067	3,045
$S(B_1)$	4,202	4,206	3,657	3,717	3,707	3,771	3,802	3,406	3,386

[a] "aXZ" stands for the aug-cc-pVXZ basis set.
[b] Ref. [42].
[c] Ref. [41].

importantly hydrogen bonds and their cooperative behavior. The work of Hirata and Iwata [47] and that of Karpfen [51] explained this point after similar discrepancies at the HF level were observed. On the inclusion of electron correlation, the structural parameters are significantly improved. The differences between CCSD and MP2 and between aug-cc-pVDZ and aug-cc-pVTZ seem rather minor as compared with those between HF and correlated results. The BSSE corrections are clearly not negligible (and they slightly weaken the hydrogen bonds) and should be included in quantitative calculations. With the aug-cc-pVTZ basis set, the corrections seem to provide improved results over the uncorrected calculations for all but certain parameters.

HARMONIC FREQUENCIES OF THE INFRARED- AND RAMAN-ACTIVE PHONONS

The calculated *harmonic* frequencies of the infrared- and/or Raman-active phonons of $(HF)_n$ and $(DF)_n$ are presented in Tables II and III, respectively. They are compared with the observed infrared band frequencies of the solid HF and DF reported by Kittelberger and Hornig [42] and the Raman band frequencies obtained by Anderson et al. [41]. The normal modes are grouped into stretching (S), librational (L), and pseudotranslational (T) modes.

In the high-frequency stretching region, the two fundamental bands assignable to the $S(A_1)$ and $S(B_1)$ modes are severely overestimated by HF. With the aug-cc-pVDZ basis set, the respective vibrational fre-

TABLE III

The harmonic frequencies (in cm^{-1}) of the infrared- and/or Raman-active vibrations of $(DF)_n$.

Mode	HF/aDZ[a]	HF/aTZ[a]	MP2/aDZ[a]	CP-MP2/aDZ[a]	MP2/aTZ[a]	CP-MP2/ aTZ[a]	CCSD/ aDZ[a]	Infrared[b]	Raman[c]
$T(A_1)$	137	135	198	176	190	183	183	210	190
$T(B_1)$	269	268	322	288	336	303	299	355	359
$L(A_1)$	372	387	400	389	450	406	383	403	417
$L(A_2)$	402	406	445	416	482	434	423	Inactive	492
$L(B_2)$	426	431	493	457	492	478	475	572	552
$L(B_1)$	557	569	722	672	703	696	688	720	703
$S(A_1)$	2,977	2,974	2,564	2,618	2,567	2,627	2,673	2,294	2,281
$S(B_1)$	3,046	3,050	2,653	2,695	2,689	2,735	2,757	2,530	2,511

[a] "aXZ" stands for the aug-cc-pVXZ basis set.
[b] Ref. [42].
[c] Ref. [41].

quencies are 4,202 and 4,106 cm^{-1}, and even with the enlarged basis (aug-cc-pVTZ), they do not much change (4,206 and 4,102 cm^{-1}). The large discrepancies of about 1,000 cm^{-1} are attributed to the underestimation of the hydrogen-bond cooperativity and vibrational anharmonicity. At the MP2 level, therefore, part of the discrepancies are removed, although not completely; the frequencies of the stretching modes are lowered, in this case, by an average of 545 cm^{-1}. On the BSSE correction, a slight increase (an average of 71 cm^{-1}) in these frequencies is observed, shifting away from the observed values, however, still offering better experimental agreement than HF. CCSD yields even higher frequencies than MP2 by about 150 cm^{-1} with the aug-cc-pVDZ basis set. The remaining errors of several 100 cm^{-1} are the basis set and anharmonic effects. In the $(DF)_n$ case (Table III), the same trends are observed with less exaggerated frequency differences. This is only a superficial improvement, as the standard deviations for $(HF)_n$ (1,531 cm^{-1}) and $(DF)_n$ (1,100 cm^{-1}) are roughly proportional to the respective stretching frequencies.

The pseudotranslational vibrations, $T(A_1)$ and $T(B_1)$, are found in the low-frequency region. Again the calculated values obtained at the HF level do not agree with the observed frequencies. They are underestimated because they are hydrogen-bond stretch and the hydrogen-bond cooperativity is too small in the HF results. The frequencies of this region calculated by MP2 and CCSD show excellent agreement with the corresponding observed data. The BSSE corrections decrease these frequencies, as expected, and are significant, but the agreement is not necessarily improved because the errors from other sources overshadow the corrections.

The librational region (1,100–500 cm^{-1}) houses the remaining four fundamental vibrational modes. The spectra in this region are rather convoluted due to the breadth of the peaks. Our HF calculations yield the frequencies of $L(A_1)$ and $L(A_2)$ that agree well with the observed values. This may only be coincidence since the two higher-frequency modes [$L(B_2)$ and $L(B_1)$] are considerably underestimated. Again, MP2 predicts the frequencies of all four librational modes in good overall agreement with the observed. Unlike the stretching modes (>3,000 cm^{-1}), the calculated frequencies of these modes tend to be lower than the observed, suggesting that they are associated with negative anharmonicity.

ANHARMONIC FREQUENCIES OF THE INFRARED- AND RAMAN-ACTIVE PHONONS

The *anharmonic* frequencies of the infrared- and/or Raman-active phonons of $(HF)_n$ were computed with the potential energy surfaces (PESs) in the one- (1MR) and two-mode coupling (2MR) approximations [24], respectively. The PESs were expressed as numerical values on rectilinear Gauss–Hermite quadrature grids in an arbitrary set of normal coordinates (11 grid points were used along each normal coordinate) and the vibrational MP2 [21–23] method as implemented in the SINDO program [54] was used. These calculations took into account only $k = 0$ phonons by scanning the PESs at geometries with in-phase nuclear displacements; in other words, the phonon dispersion was ignored. The 1MR CCSD(T)/aug-cc-pVDZ calculations were carried out using the CCSD/aug-cc-pVDZ optimized geometry, harmonic frequencies, and normal coordinates. In the 2MR CCSD(T)+MP2/

TABLE IV

The anharmonic frequencies (in cm^{-1}) of the infrared- and/or Raman-active vibrations of $(HF)_n$ obtained by vibrational MP2 within the 1 MR PESs.

Mode	HF/aDZ[a]	HF/aTZ[a]	MP2/aDZ[a]	CP-MP2/aDZ[a]	MP2/aTZ[a]	CP-MP2/aTZ[a]	CCSD/aDZ[a]	CCSD(T)/aDZ[a]	Infrared[b]	Raman[c]
$T(A_1)$	127	125	187	169	172	174	170	171	202	188
$T(B_1)$	287	285	340	306	355	319	343	343	356	364
$L(A_1)$	753	764	747	729	792	754	753	732	553	569
$L(A_2)$	777	782	782	752	840	778	788	769	Inactive	687
$L(B_2)$	806	812	831	791	826	821	810	785	792	742
$L(B_1)$	914	927	1,058	1,002	1,042	1,038	1,001	981	975-1,025	943
$S(A_1)$	3,896	3,894	3,184	3,344	3,172	3,295	3,350	3,278	3,067	3,045
$S(B_1)$	4,318	4,318	3,814	3,866	3,815	3,873	3,906	3,899	3,406	3,386

[a] "aXZ" stands for the aug-cc-pVXZ basis set.
[b] Ref. [42].
[c] Ref. [41].

TABLE V

The anharmonic frequencies (in cm^{-1}) of the infrared- and/or Raman-active vibrations of $(HF)_n$ obtained by vibrational MP2 with the 2MR PESs.

Mode	HF/aDZ[a]	MP2/aDZ[a]	CCSD(T)+MP2/aDZ[b]	Infrared[c]	Raman[d]
$T(A_1)$	116	183	184	202	188
$T(B_1)$	291	380	377	356	364
$L(A_1)$	560	658	647	553	569
$L(A_2)$	599	719	704	Inactive	687
$L(B_2)$	631	749	741	792	742
$L(B_1)$	767	1,012	1,000	975-1,025	943
$S(A_1)$	3,816	3,007	3,096	3,067	3,045
$S(B_1)$	3,718	3,091	3,166	3,406	3,386

[a] "aXZ" stands for the aug-cc-pVXZ basis set.
[b] The 1MR and 2MR parts of the PESs were obtained by CCSD(T)/aug-cc-pVDZ and MP2/aug-cc-pVDZ, respectively.
[c] Ref. [42].
[d] Ref. [41].

aug-cc-pVDZ calculations, we combined 1MR CCSD(T) and 2MR MP2 PESs, which were both expressed in terms of the MP2/aug-cc-pVDZ geometry and normal coordinates.

Table IV lists the anharmonic frequencies in the 1MR approximation. The frequencies of the $S(A_1)$ and $S(B_1)$ modes are affected differently by anharmonicity. The $S(A_1)$ mode is an in-phase H–F stretch and the potential energy curve along this mode is strongly Morse-like. Consequently, there is a large decrease (by 300–350 cm^{-1}) in the frequency on going from a harmonic to anharmonic treatment. The benefits of anharmonicity on the $S(B_1)$ mode, an out-of-phase H–F stretch, on the other hand, are somewhat less. Its anharmonic frequency is larger than the harmonic counterpart (by 100–150 cm^{-1}). The pseudotranslational modes are affected similarly as the H–F stretching modes. The frequencies of $T(A_1)$, which can be viewed as an in-phase stretch of the hydrogen bonds, are lowered by the inclusion of the anharmonicity, whereas the $T(B_1)$ frequencies (out-of-phase stretch) increase slightly (by about 10 cm^{-1}). The librational modes increase their frequencies upon inclusion of anharmonicity in the direction of the experimental values (the negative anharmonicity). However, the increases tend to be too large and the anharmonic frequencies are significantly overestimated. Consequently, the mean absolute deviation from the Raman measurements (156 cm^{-1}) of the highest-level calculation (CP-MP2/aug-cc-pVTZ) is slightly greater than the harmonic counterpart (125 cm^{-1}).

Table V attests to the dramatic improvements in the anharmonic frequencies brought to by the 2MR

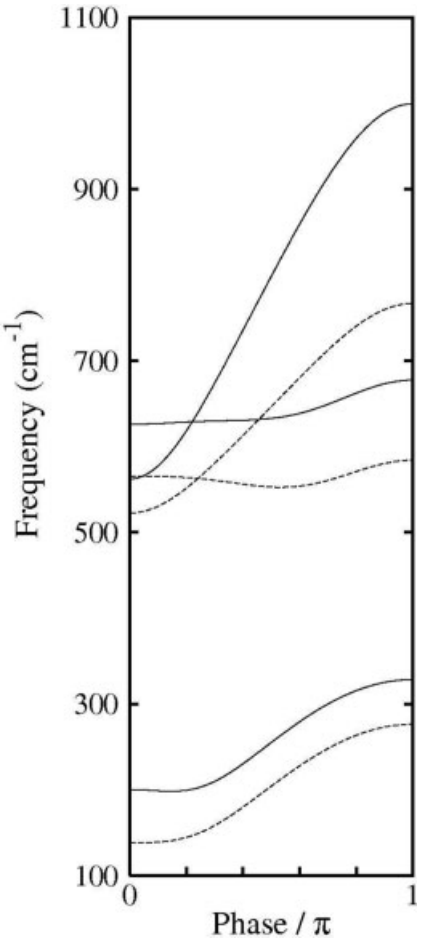

FIGURE 1. The optical phonon dispersion curves (100–1,100 cm^{-1}) of $(HF)_n$ obtained by MP2 (solid curves) and HF (broken curves) with the aug-cc-pVDZ basis set. The abscissa is the phase difference between the two adjacent HF oscillators.

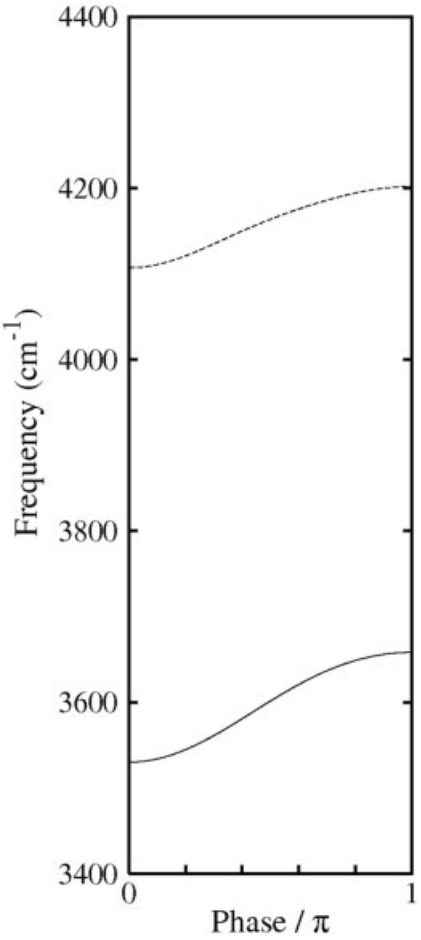

FIGURE 2. The optical phonon dispersion curves (3,400–4,400 cm^{-1}) of $(HF)_n$ obtained by MP2 (solid curves) and HF (broken curves) with the aug-cc-pVDZ basis set. The abscissa is the phase difference between the two adjacent HF oscillators.

treatment. The $S(A_1)$ frequencies are lowered by another 80–180 cm^{-1} relative to the 1MR results and become closer to the experimental values. The $S(B_1)$ frequencies, which were hardly improved by the 1MR treatment, are now reduced by as much as 600–730 cm^{-1}. These shifts may be too large, but they nevertheless bring theory and experiment in slightly better accord. The frequencies of $T(B_1)$ are raised by the 2MR somewhat, again improving the agreement. The librational modes, for which the 1MR anharmonic calculations are most troublesome, undergo systematic and noticeable improvements upon inclusion of the anharmonic mode-mode couplings at the 2MR. The best overall agreement is obtained between the combined CCSD(T) and MP2 calculation and the Raman measurement with the mean absolute deviation of 55 cm^{-1}, which is 2–3 times smaller than the corresponding harmonic and 1MR anharmonic values. The results underscore the significance of anharmonic mode-mode coupling among phonons. They render a further support to the aforementioned assignments of the librational modes.

PHONON DISPERSIONS AND INELASTIC NEUTRON SCATTERING

The optical phonon dispersion curves of $(HF)_n$ are depicted in Figures 1 and 2 and those of $(DF)_n$ in Figures 3 and 4. The infrared- and Raman-active vibrations occur at the edges of the curves. Our calculations show a large dispersion in the high-

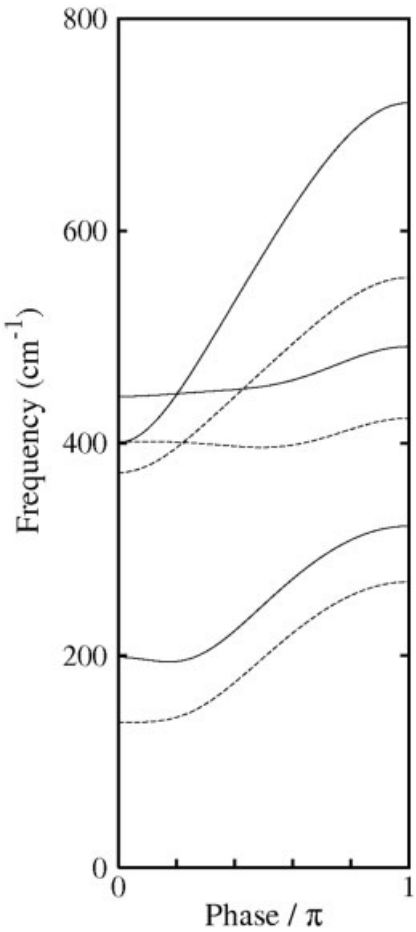

FIGURE 3. The optical phonon dispersion curves (0–800 cm^{-1}) of $(DF)_n$ obtained by MP2 (solid curves) and HF (broken curves) with the aug-cc-pVDZ basis set. The abscissa is the phase difference between the two adjacent DF oscillators.

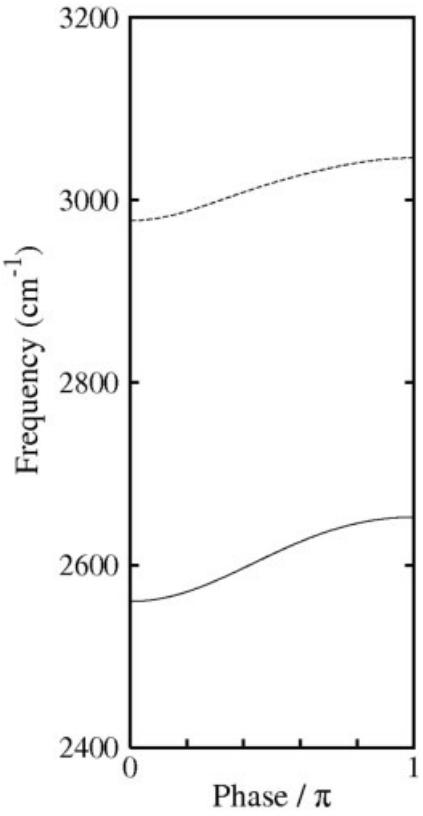

FIGURE 4. The optical phonon dispersion curves (2,400–3,200 cm^{-1}) of $(DF)_n$ obtained by MP2 (solid curves) and HF (broken curves) with the aug-cc-pVDZ basis set. The abscissa is the phase difference between the two adjacent DF oscillators.

frequency stretching $S(A_1)$-$S(B_1)$ branch as well as in the pseudotranslational $T(A_1)$-$T(B_1)$ branch. Both of these branches correspond to the motions along the chain axis. The librational region shows a large dispersion in the $L(A_1)$-$L(B_1)$ branch. This is in disagreement obviously with the results of Tubino and Zerbi [55], which show only small dispersions in the librational region; however, the work of Beyer and Karpfen [48] suggests that both dispersions in this region are rather large, particularly the $L(A_1)$-$L(B_1)$ branch. A comparison between the MP2 and HF branches indicates that electron correlation merely shifts the curves either upward or downward but the shapes are almost unchanged.

The hydrogen-amplitude-weighted phonon density of states and simulated INS spectrum of $(HF)_n$ are displayed in Figure 5. The experimental INS spectrum of Boutin et al. [56] shows two peaks at 53 and 539 cm^{-1} and a low intensity shoulder at 216 cm^{-1}. Axmann et al. [57] observed a total of five peaks: two sharp ones at 57 and 605 cm^{-1} and three more at 87, 133, and 223 cm^{-1}. Our predicted spectrum exhibits peaks clustering around 30 cm^{-1}, another two peaks centered at 240 cm^{-1}, and some very intense peaks starting at 550 cm^{-1}. Clearly, the observed peak at 53–57 cm^{-1} is assigned to the cluster at around 30 cm^{-1}, which are due to acoustic phonons not shown in Figure 1. A small peak at 216 or 223 cm^{-1} corresponds to the $T(A_1)$ mode, giving rise to the infrared and Raman bands at about 200 cm^{-1}. The peaks at 550 to 605 cm^{-1} are contributed chiefly by $L(A_1)$ and by the $L(A_2)$-$L(B_2)$ branch.

Conclusions

We have studied $(HF)_n$ and $(DF)_n$ with our binary-interaction method under the periodic boundary conditions. The optimized structural parameters and harmonic frequencies of the $k = 0$ phonons obtained by HF have large errors because of the inability of the HF theory to describe the cooperative behavior of network hydrogen bonds. MP2 and CCSD yield the structural properties and harmonic frequencies that agree with the experimental values considerably more accurately, although some errors still remain that are probably due to basis set deficiencies. The anharmonic calculations in the 1MR treatment, which includes only single-mode anharmonicity but no mode-mode coupling, do not improve the overall agreement, while they certainly improve the $S(A_1)$ frequencies. The inclusion of anharmonic mode-mode couplings at least in the

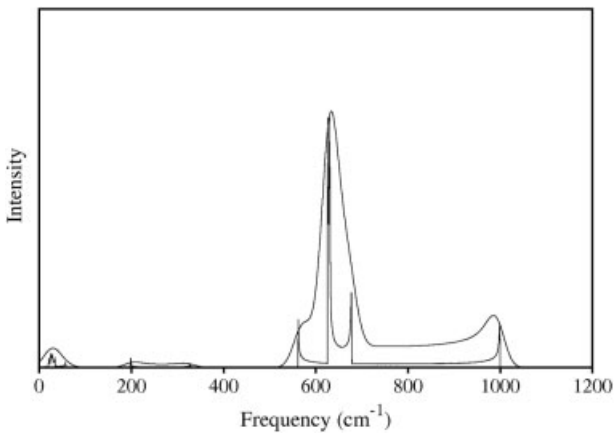

FIGURE 5. The hydrogen-amplitude-weighted density of states (the histogram) and its Gaussian convolution (with a FWHM of 40 cm^{-1}) as a simulated INS spectrum of $(HF)_n$.

2MR dramatically reduces the errors in calculated frequencies, underscoring the significance of such couplings among phonons. The phonon dispersion curves computed at the MP2 level supported the revised infrared and Raman band assignments of Hirata and Iwata [47] and the prediction of Beyer and Karfpen [48]: the L(B_1) mode having the highest frequency among the librational modes and a large dispersion in the L(A_1)-L(B_1) branch. Our simulated INS spectrum reproduces the features of the observed spectra and their assignments. The ease of implementation and use of this method in conjunction with any electron-correlation theory renders this proposed method with a great promise as a general ab initio tool for structure and property prediction of molecular crystals.

ACKNOWLEDGMENTS

Two of the authors (S.H. and K.Y.) express their heartfelt gratitude to the continuous encouragement and passionate career support Professor Kimihiko Hirao has provided with them for many years and his strong leadership in promoting the field of theoretical chemistry in Japan and globally. They have also been privileged to work with Kimihiko on numerous joint research projects and inspired by his profound insight and knowledge in electronic structures and dynamics. K.Y. thanks the Grant-in-Aid for Scientific Research (KAKENHI) on Priority Areas "Molecular Science for Supra Functional Systems" [477] from MEXT, Japan.

References

1. Maddox, J. Nature 1988, 335, 201.
2. Del Re, G.; Ladik, J.; Biczó, G. Phys Rev 1967, 155, 997.
3. André, J. M. J Chem Phys 1969, 50, 1536.
4. Kertész, M. Adv Quantum Chem 1982, 15, 161.
5. Ladik, J. J. Quantum Theory of Polymers as Solids; Plenum: New York, 1988.
6. Sun, J. Q.; Bartlett, R. J. Topics Curr Chem 1999, 203, 121.
7. Hirata, S.; Podeszwa, R.; Tobita, M.; Bartlett, R. J. J Chem Phys 2004, 120, 2581.
8. Hirata, S.; Valiev, M.; Dupuis, M.; Xantheas, S. S.; Sugiki, S.; Sekino, H. Mol Phys 2005, 103, 2255.
9. Kamiya, M.; Hirata, S.; Valiev, M. J Chem Phys 2008, 128, 074103.
10. Hirata, S. J Chem Phys 2008, 129, 204104.
11. Atoji, M.; Lipscomb, W. N. Acta Cryst 1954, 7, 173.
12. Johnson, M. W.; Sándor, E.; Arzi, E. Acta Cryst B 1975, 31, 1998.
13. Sastri, M. L. N.; Hornig, D. F. J Chem Phys 1963, 39, 3497.
14. Del Bene, J. E.; Pople, J. A. J Chem Phys 1970, 52, 4858.
15. Del Bene, J. E.; Pople, J. A. J Chem Phys 1971, 55, 2296.
16. Del Bene, J. E.; Pople, J. A. J Chem Phys 1973, 58, 3605.
17. Schuster, P.; Zundel, G.; Sandorfy, C. The Hydrogen Bond; North Holland: Amsterdam, 1976.
18. Jeffrey, G. A.; Gress, M. E.; Takagi, S. J Am Chem Soc 1977, 99, 609.
19. Tse, Y. C.; Newton, M. D. J Am Chem Soc 1977, 99, 611.
20. Jeffrey, G. A.; Saenger, W. Hydrogen Bonding in Biological Structures; Springer-Verlag: Berlin, 1991.
21. Norris, L. S.; Ratner, M. A.; Roitberg, A. E.; Gerber, R. B. J Chem Phys 1996, 105, 11261.
22. Christiansen, O. J Chem Phys 2003, 119, 5773.
23. Yagi, K.; Hirata, S.; Hirao, K. J Chem Phys 2007, 127, 034111.
24. Carter, S.; Culik, S. J.; Bowman, J. M. J Chem Phys 1997, 107, 10458.
25. Shao, Y.; Molnar, L. F.; Jung, Y.; Kussmann, J.; Ochsenfeld, C.; Brown, S. T.; Gilbert, A. T. B.; Slipchenko, L. V.; Levchenko, S. V.; O'Neill, D. P.; DiStasio, R. A.; Lochan, R. C.; Wang, T.; Beran, G. J. O.; Besley, N. A.; Herbert, J. M.; Lin, C. Y.; Van Voorhis, T.; Chien, S. H.; Sodt, A.; Steele, R. P.; Rassolov, V. A.; Maslen, P. E.; Korambath, P. P.; Adamson, R. D.; Austin, B.; Baker, J.; Byrd, E. F. C.; Dachsel, H.; Doerksen, R. J.; Dreuw, A.; Dunietz, B. D.; Dutoi, A. D.; Furlani, T. R.; Gwaltney, S. R.; Heyden, A.; Hirata, S.; Hsu, C. P.; Kedziora, G.; Khalliulin, R. Z.; Klunzinger, P.; Lee, A. M.; Lee, M. S.; Liang, W.; Lotan, I.; Nair, N.; Peters, B.; Proynov, E. I.; Pieniazek, P. A.; Rhee, Y. M.; Ritchie, J.; Rosta, E.; Sherrill, C. D.; Simmonett, A. C.; Subotnik, J. E.; Woodcock, H. L.; Zhang, W.; Bell, A. T.; Chakraborty, A. K.; Chipman, D. M.; Keil, F. J.; Warshel, A.; Hehre, W. J.; Schaefer, H. F.; Kong, J.; Krylov, A. I.; Gill, P. M. W.; Head-Gordon, M. Phys Chem Chem Phys 2006, 8, 3172.
26. Straatsma, T. P.; Aprà, E.; Windus, T. L.; Dupuis, M.; Bylaska, E. J.; de Jong, W.; Hirata, S.; Smith, D. M. A.; Hackler, M. T.; Pollack, L.; Harrison, R. J.; Nieplocha, J.; Tipparaju, V.; Krishnan, M.; Auer, A. A.; Brown, E.; Cisneros, G.; Fann, G. I.; Fruchtl, H.; Garza, J.; Hirao, K.; Kendall, R.; Nichols, J. A.; Tsemekhman, K.; Valiev, M.; Wolinski, K.; Anchell, J.; Bernholdt, D.; Borowski, P.; Clark, T.; Clerc, D.; Dachsel, H.; Deegan, M.; Dyall, K.; Elwood, D.; Glendening, E.; Gutowski, M.; Hess, A.; Jaffe, J.; Johnson, B.; Ju, J.; Kobayashi, R.; Kutteh, R.; Lin, Z.; Littlefield, R.; Long, X.; Meng, B.; Nakajima, T.; Niu, S.; Rosing, M.; Sandrone, G.; Stave, M.; Taylor, H.; Thomas, G.; van Lenthe, J.; Wong, A.; Zhang, Z. Pacific Northwest National Laboratory: Richland, WA, 2003.
27. Kitaura, K.; Sugiki, S.-I.; Nakano, T.; Komeiji, Y.; Uebayasi, M. Chem Phys Lett 2001, 336, 163.
28. Teramae, H.; Yamabe, T.; Imamura, A. J Chem Phys 1984, 81, 3564.
29. Boys, S. F.; Bernardi, F. Mol Phys 1970, 19, 553.
30. Kitaura, K.; Sawai, T.; Asada, T.; Nakano, T.; Uebayasi, M. Chem Phys Lett 1999, 312, 319.
31. Tschumper, G. S. Chem Phys Lett 2006, 427, 185.
32. Dahlke, E. E.; Truhlar, D. G. J Chem Theor Comp 2007, 3, 46.
33. Dahlke, E. E.; Truhlar, D. G. J Chem Theor Comp 2007, 3, 1342.
34. Li, S. H.; Shen, J.; Li, W.; Jiang, Y. S. J Chem Phys 2006, 125, 074109.
35. Jiang, N.; Ma, J.; Jiang, Y. J Chem Phys 2006, 124, 114112.
36. Stoll, H.; Paulus, B.; Fulde, P. J Chem Phys 2005, 123, 144108.

37. Manby, F. R; Alfè, D.; Gillan, M. J. Phys Chem Chem Phys 2006, 8, 5178.
38. Podeszwa, R.; Rice, B. M.; Szalewicz, K. Phys Rev Lett 2008, 101, 115503.
39. Ringer, A. L.; Sherrill, C. D. Chem Eur J 2008, 14, 2542.
40. Giguère, P. A.; Zengin, N. Can J Chem 1958, 36, 1013.
41. Anderson, A.; Torrie, B. H.; Tse, W. S. Chem Phys Lett 1980, 70, 300.
42. Kittelberger, J. S.; Hornig, D. F. J Chem Phys 1967, 46, 3099.
43. Lee, S. A.; Pinnick, D. A.; Lindsay, S. M.; Hanson, R. C. Phys Rev B 1986, 34, 2799.
44. Jansen, R. W.; Bertoncini, R.; Pinnick, D. A.; Katz, A. I.; Hanson, R. C.; Sankey, O. F.; Okeeffe, M. Phys Rev B 1987, 35, 9830.
45. Pinnick, D. A.; Katz, A. I.; Hanson, R. C. Phys Rev B 1989, 39, 8677.
46. Habuda, S. P.; Gagarinsky, Y. V. Acta Crystallogr B 1971, 27, 1677.
47. Hirata, S.; Iwata, S. J Phys Chem A 1998, 102, 8426.
48. Beyer, A.; Karpfen, A. Chem Phys 1982, 64, 343.
49. Buth, C.; Paulus, B. Chem Phys Lett 2004, 398, 44.
50. Buth, C.; Paulus, B. Phys Rev B 2006, 74, 045122.
51. Karpfen, A. In Molecular Interactions; Scheiner, S., Ed.; Wiley: Chichester, 1997; p 265.
52. Yagi, K.; Taketsugu, T.; Hirao, K. J Chem Phys 2002, 116, 3963.
53. Yagi, K.; Hirao, K.; Taketsugu, T.; Schmidt, M. W.; Gordon, M. S. J Chem Phys 2004, 121, 1383.
54. Yagi, K. University of Tokyo: Tokyo, Japan, 2006.
55. Tubino, R.; Zerbi, G. J Chem Phys 1969, 51, 4509.
56. Boutin, H.; Safford, G. J.; Brajovic, V. J Chem Phys 1963, 39, 3135.
57. Axmann, A.; Biem, W.; Borsch, P.; Hossfeld, F.; Stiller, H. Discuss Faraday Soc 1969, 48, 69.